ELSEVIER

Available online at www.sciencedirect.com

SCIENCE DIRECT®

Microelectronic Engineering 71 (2004) 76–89

MICROELECTRONIC ENGINEERING

www.elsevier.com/locate/mee

Effects of mechanical stress at no current stressed area on electromigration reliability of multilevel interconnects

Young-Bae Park [a,*], In-Su Jeon [b,1]

[a] *School of Materials Science and Engineering, Andong National University, Andong 760-749, South Korea*
[b] *PKG & Module R&D Center, Hynix semiconductor Inc., Ichon 467-701, South Korea*

Received 16 April 2003; received in revised form 1 August 2003; accepted 17 September 2003

Abstract

Reservoir length dependencies of electromigration lifetime in multilevel interconnect were compared for two passivation dielectrics, i.e., flowable oxide (FOX) and high density plasma fluorinated silicate glass (HDP FSG). These results were analyzed mainly by both X-ray diffraction (XRD) and finite element method (FEM) for determination of the mechanical stress in Al–Cu interconnect lines. Also, it was utilized the mathematical calculation for the vacancy concentration distribution in the reservoir region. The higher electromigration resistance of interconnects passivated by FOX than those passivated by FSG could be best explained by the large stiffness difference which caused different constraint in the Al line during the electromigration when mechanical stresses and stress gradients were building up. It was also proposed that lower levels of stress and vacancy concentration in the longer reservoir could partially contribute to the better electromigration reliability of interconnect.
© 2003 Elsevier B.V. All rights reserved.

Keywords: Electromigration; Al–Cu interconnect; Reservoir length; Mechanical stress; Passivation dielectric

1. Introduction

Mechanical stress in metal interconnect line is very important in large scale device integration because the metal line is mostly under a triaxial stress state, i.e., favorable for void formation which is a major concern for the reliability of multi-level metallization [1,2]. The incorporation of several levels of metallization and passivation in an integrated circuit device exposes the interconnects to multiple thermal cycles as much as 400 °C. High tensile stresses evolve in the metal lines during the cooling process from the passivation temperature by the thermal expansion mismatches with the surrounding dielectrics and Si substrate. These triaxial tensile stresses that arise within the metal lines facilitate void formation, which can eventually cause the failure of devices [1,2]. In

* Corresponding author. Tel.: +82-54-820-5121; fax: +82-54-820-5121.

E-mail addresses: ybpark@andong.ac.kr (Y.-B. Park), i_jeon@ichizai-7.mep.titech.ac.jp (I.-S. Jeon).

[1] Present address: Department of Mechanical and Control Engineering, Tokyo Institute of Technology, Ishikawadai 1-204, 2-12-1 O-okayama, Meguro-ku, Tokyo 152-8552, Japan. Tel.: +81-3-5734-2783; fax: +81-3-5734-3917.

0167-9317/$ - see front matter © 2003 Elsevier B.V. All rights reserved.
doi:10.1016/j.mee.2003.09.004

addition to this direct stress-induced voiding problem, electromigration-induced voiding is also strongly influenced by the mechanical stress evolution within metal lines, especially at no current stressed region (especially, a reservoir which can be defined as an extended region of metal line under or over via) in multilevel interconnect structure [3–5]. Moreover, dielectric passivation on metal interconnect can significantly change the stress-state in the metal line [6–9]. Different stress states in the conductor lines by different passivation materials would strongly influence the electromigration-induced voiding [10,11]. Therefore, thorough understanding, precise measurement, and control of stress evolution in metal interconnects are essential for electromigration reliability of multi-level metallization structure.

The main cause of electromigration failure in multilevel interconnect structure is the flux divergence of Al atom flow at the interface between Al line and W plug. Voids are formed due to Al depletion near the contact area of W via with Al line. It has been reported that a reservoir contributes to the improvement of electromigration reliability in multi-level metallization structure because it can compensate the electromigrated Al atoms [3,4]. It is very interesting that reservoir can affect the electromigration reliability even though there is no current flow in it. Dominant mechanism for the void formation at reservoir region is thought to be that vacancies induced by the flux divergence of Al atom near the interface between Al line and W plug diffuse toward the regions of lower vacancy concentration (i.e., inside of reservoir) due to the spatial gradient of vacancy concentration [3–5]. It was also simply mentioned without evidence that vacancies induced by electromigration caused mechanical stress gradient and diffused toward edge of reservoir for stress relaxation [3]. Although the effect of mechanical stress evolution on void formation in reservoir region and on electromigration reliability of multilevel metallization structure is very important, there were few detailed reports on this issue.

In this paper, we reported the results of a systematic experimental and computational analysis on the effects of reservoir length and passivation material not only on the distributions of both mechanical stress and vacancy concentration in reservoir region, but also on the electromigration reliability of multilevel interconnect structure. Reservoir length (0.04–0.30 μm) dependencies of electromigration lifetime of multilevel interconnect were compared for two passivation dielectrics, i.e., FOX and FSG. Direct XRD determination of the mechanical stress in Al–Cu interconnect lines was carried out at narrow metal line width/space condition for above two passivation dielectrics. Young's modulus and residual stress of each constituent layer of our multilevel interconnect structure were measured by nanoindentation and wafer curvature method, respectively. Both finite element analysis and focused ion beam failure analysis for our test structure were performed to reveal the effects of mechanical stress evolution on not only voiding phenomena but also electromigration reliability for various reservoir lengths and passivation dielectrics. Finally, possible mechanisms for passivation dielectric and reservoir length dependencies of electromigration lifetime of multilevel interconnect were discussed.

2. Experimental and numerical procedures

Electromigration test structure with two-level metallization as shown in Fig. 1 was fabricated using the procedure described below. Plasma enhanced chemical vapor deposited (PECVD) oxide of 700 nm was prepared on P-type ⟨1 0 0⟩ Si wafer. A bottom-Ti (10 nm)\Al – 0.5%Cu (350 nm)\Ti (5 nm)\TiN (60 nm)-top stack was then deposited using a multi-chamber dc magnetron sputtering system without vacuum break. That is, 10 nm of Ti was deposited, which was followed by in-situ sputter deposition of 350 nm of Al – 0.5%Cu with process power of 12 kW at 400 °C. On the top of Ti\Al structure, 5 nm of Ti and 60 nm of TiN were deposited in a single chamber. This caused the formation of a very thin Ti–N layer at the interface between the Al and top-Ti because the surface of Ti target was slightly nitrized due to the previous top-TiN deposition using a pure Ti target in mixed atmosphere of Ar–N_2 [12]. The metal stack was then patterned by standard photolithography and

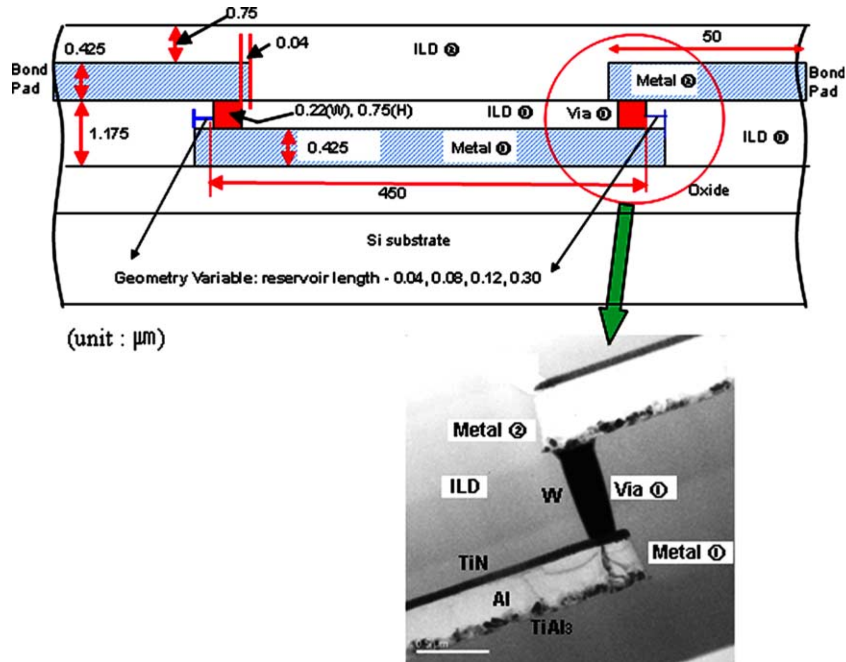

Fig. 1. Schematic geometry and cross-sectional TEM photograph of two-level metallization structure used in the electromigration test.

plasma dry etching. Either FSG or FOX was deposited on the patterned metal lines. This was followed by deposition of plasma enhanced tetraethyl ortho silicate (PETEOS) film and then planarization by chemical–mechanical polishing (CMP), which results in inter-level dielectric (ILD) of either FSG\PETEOS or FOX\PETEOS. After via hole opening and Ar sputter etching were carried out, via plugs were fabricated by in situ deposition of Ti\TiN liner, CVD W deposition, and W CMP. The same processes were repeated to make the second level structure and finally pad for wire bonding to package was opened by patterning process. A cross-sectional transmission electron microscope (TEM) photograph near via 1 of electromigration test structure was shown in Fig. 1. It could be seen that Ti–Al reaction layer ($TiAl_3$) was formed uniformly across the bottom-Ti\Al interface while no reaction was observed at Al\-top-Ti (slightly nitrized) interface by the reason mentioned above [12]. Metal 1 layer consisted of 0.2 μm wide, 0.425 μm thick and 450 μm long straight line. Metal 2 layer consisted of 0.24 μm wide, 0.425 μm thick and 50 μm long straight line connected with bonding pad for chip packaging. Reservoir length of metal 2 (or, metal 2 extension over via 1) was constant by 0.04 μm and reservoir length of metal 1 (or, metal 1 extension under via 1) was varied by 0.04, 0.08, 0.12, and 0.30 μm. ILD structures were compared between FSG\PETEOS and FOX\PETEOS. Wafers were annealed for 50 min at 400 °C in a forming gas (N_2/H_2) ambient for stabilization of microstructure before an accelerated electromigration testing. In the package-level electromigration test, ambient temperature and current density were 200 °C and 2 MA/cm^2, respectively. The current density was calculated from the cross-sectional area of metal 1 line. Failure criterion was defined as an increase in resistance above either 3% or 20%. Metal 1 line end region of cathode direction was analyzed before and after electromigration test by cross-sectional TEM to compare voiding characteristics with the variations of ILD material and reservoir length. Young's modulus and residual stress of every constituent layer of 450 nm thickness used in this electromigration test structure were measured on Si wafer by nanoindentation method [13] and

wafer curvature method, respectively. Data measured at five different positions of each sample were averaged to give Young's modulus of each layer. XRD experiment was done with monocromated Cu K_α beam, at 40 kV and 100 mA conditions. The X-ray beam was aligned to expose the center of a 4×4 mm^2 square block composed of uniform line and space patterns having 0.25 μm width (*w*), 0.25 μm space (*s*), 0.425 μm height (*h*, thickness of Ti\Al–Cu\Ti\TiN stack), and 4000 μm length, which resulted in aspect ratio (w/h) of 0.6. By the well-established technique [14,15], triaxial stress components of Al in metal stack (bottom-Ti\Al – 0.5%Cu\Ti\TiN-top) passivated by either FSG or FOX were obtained in length (*x*), width (*y*), and height (*z*) direction, separately, from the measured XRD data.

The general purpose finite element program ABAQUS [16] was used to calculate the stress distributions in the model structure under the assumptions of a good adhesion between dissimilar materials, and a uniform temperature distribution in the model structure at each temperature step. In addition, stress-free state of the model was assumed to be the ILD deposition temperature (400 °C). The intrinsic stress of each constituent material was ignored based on the assumption that it can be considered to have been fully relaxed at the ILD deposition temperature, which was revealed in some earlier works [1,2,6]. Therefore, the stress calculated in this study was the thermal stress induced by the thermal expansion mismatches between dissimilar materials at various temperatures. Eight-noded isoparametric plane strain elements were used to make up the finite element mesh. In the calculations, only the right half of the structure was modeled, due to symmetry, as shown in Fig. 2, where metal 1 reservoir length varied by 0.04, 0.08, 0.12, and 0.30 μm while metal 2 reservoir length was constant by 0.04 μm. For the boundary conditions of this model, the symmetric condition was applied on the left edge. X- and Y-direction constraints were loaded on the right and bottom edge, respectively.

Al–Cu was assumed to behave as an elastic-plastic material while the other layers were assumed to show a linear-elastic behavior. Temperature-dependent material properties were also used for

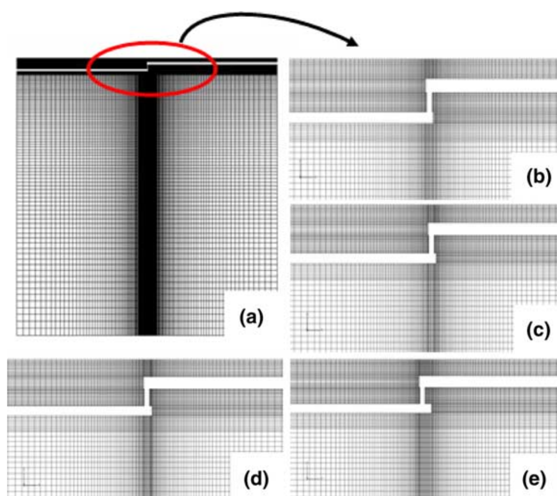

Fig. 2. Finite element mesh of (a) right half of overall structure; magnification near via with metal 1 reservoir length of (a) 0.04, (b) 0.08, (c) 0.12, and (d) 0.30 μm, where, white region in each figure means metal interconnect.

Al–Cu [2,7–9]. Table 1 summarized the material properties used in this simulation where each value of Young's modulus at room temperature was measured by nanoindentation method. By lack of mechanical property data of thin (∼60 nm) $TiAl_3$ layer formed under Al–Cu line (cf. Fig. 1), we used the measured Young's modulus of TiN as that of $TiAl_3$ in finite element simulation. The temperature excursion was conducted by cooling the model from ILD deposition temperature (400 °C: stress-free temperature) to room temperature (20 °C) and then heating to electromigration test temperature (200 °C). The stress distribution was then calculated from the resulting state. Because of the material nonlinearities due to the elastic–plastic behavior of Al–Cu metal line, the finite-element solution was obtained through iteration until a criterion for convergence was satisfied.

3. Results and discussion

3.1. Electromigration reliability

Electromigration lifetimes of two-level metallization structure shown in Fig. 1 were compared for ILD variations (FOX\TEOS vs. FSG\TEOS)

Table 1
Material properties used in the finite element analysis

Material	E^a (GPa)	v	CTE (ppm/K)	Yield stress (MPa)
Si	145	0.26	2.6	
Al–Cu	$59 - 0.04(T - 20)$	0.34	$24.3 + 0.02(T - 20)$	$200 - 0.35(T - 20)$
FSG	51	0.19	3	
FOX	8	0.19	20.5	
PETEOS	75	0.24	1	
TiN	270	0.25	9.4	
Ti	140	0.25	8.9	
W	411	0.28	4.5	

[a] Measured by nanoindentation method.

and metal 1 reservoir length variations (0.04, 0.08, 0.12, and 0.30 μm). Fig. 3 showed the cumulative percentage of the time to failure, for either 3% or 20% failure criteria, respectively, and Table 2 summarized not only the electromigration test results of Fig. 3 but also the blanket Al film microstructures obtained in our previous works [12]. The microstructure of Al interconnect would be bamboo structure because the line width of 0.2 μm was well below the median grain size of blanket Al film (cf. Table 2). The measured joule-heating temperatures were under 5 °C

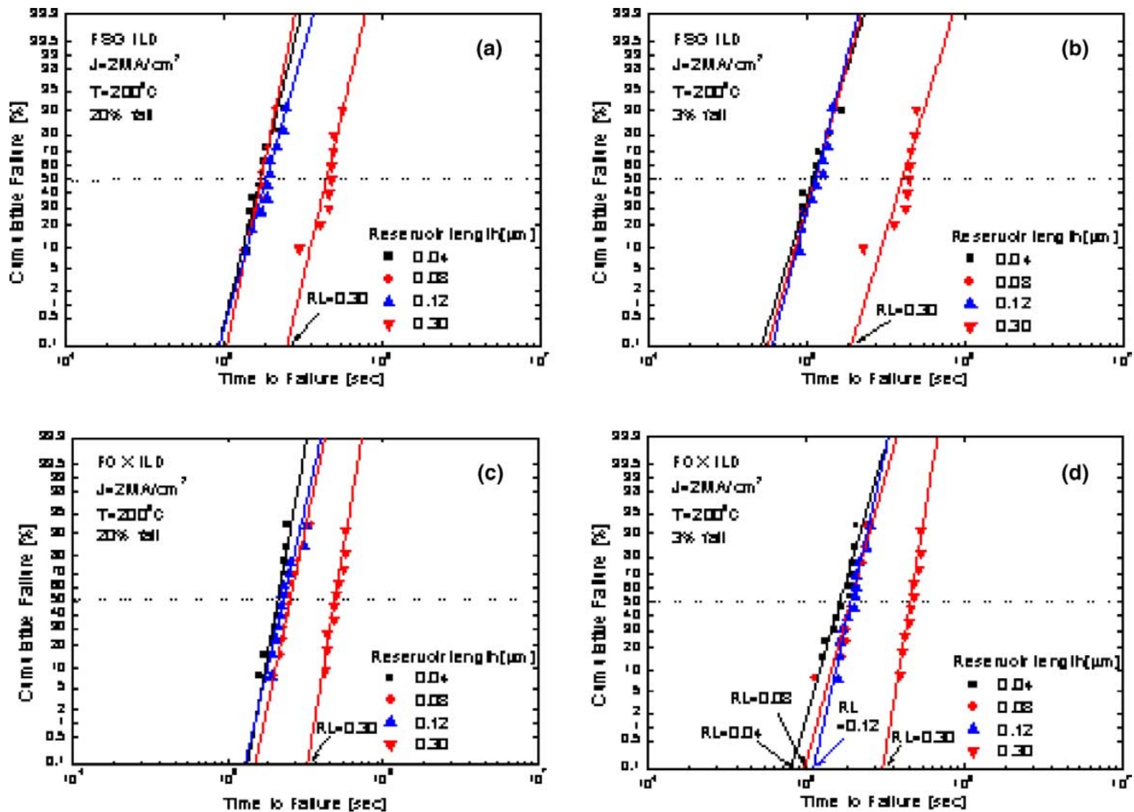

Fig. 3. Cumulative percentage of the time to failure of Al stacks as a function of metal 1 reservoir length (RL) for failure criteria and ILD of (a) 20% and FSG, (b) 3% and FSG, (c) 20% and FOX, and (d) 3% and FOX, respectively.

Table 2
Summary of Al stack microstructures and electromigration test results as a function of reservoir length and ILD material

Reservoir length (μm)	FWHM of Al (1 1 1) (°)[a]	Al grain size distribution		Electromigration lifetime[d]			
		S^b (μm)	σ^c	FSG		FOX	
				MTTF (h)	σ	MTTF (h)	σ
0.04	2.1	0.73	0.52	48.0	0.19	58.6	0.14
0.08				48.6	0.16	70.6	0.16
0.12				52.3	0.22	63.9	0.18
0.30				126.3	0.18	137.3	0.13

[a,b,c] Ref. [12].
[b] Median grain size.
[c] Log-normal standard deviation.
[d] At 20% resistance increase, 200 °C, and $J = 2$ MA/cm^2.

at 200 °C and 2 MA/cm^2 conditions for either FSG or FOX. Mean time to failure (MTTF) and log-normal standard deviation (σ) were obtained from a best-fit straight line drawn through data points in the log-normal plot of time to failure, as shown in Fig. 3. MTTF was given by the intercept at the 50% cumulative failure point (t_{50}), and σ was defined as $\log(t_{50}/t_{16})$. Time for 0.1% cumulative failure ($t_{0.1}$) could be defined as electromigration lifetime [12]. MTTF for FOX was longer than that for FSG and σ seemed to be similar for both cases, which resulted in the longer $t_{0.1}$ for FOX than FSG. It was also clearly shown that the electromigration reliability improved much better for the via with larger reservoir (0.3 μm). Reservoir length dependence of electromigration lifetime for smaller size ranges (0.04, 0.08, and 0.12 μm) was not clear for FSG but a little clear for FOX. Also, there was little difference in trends between 3% and 20% failure criteria, which represented that voiding mechanism did not vary significantly during resistance increase from 3% to 20%.

To compare electromigration-failed void morphologies with the variation of ILD materials and reservoir lengths, metal 1 line end region of cathode direction was analyzed by cross-sectional TEM after resistance increase of 20%, which is shown for FSG in Fig. 4. It could be seen that Al voids formed from the reservoir edge and extended across the via interface, while both bottom-$TiAl_3$ and top-TiN layers were conserved in shape, where electrons flowed from metal 2 to metal 1 regardless of reservoir length. There was little difference in void morphologies between FSG and FOX. Electromigration-induced voiding in multilevel interconnect is known to occur by Al atom depletion near the contact area of W via with Al line which is caused by large Al atomic flux divergence near the W/Al interface along electric current path [3–5]. However, when there is a reservoir region at the metal line end as in this study, this mechanism can not fully explain the voiding morphology that extended to reservoir edge where there is no current flow. From our electromigration test results (cf. Fig. 3) and TEM failure analysis results (cf. Fig. 4), it could be seen that Al atoms in the reservoir area were mostly depleted and then the resistance of this structure increased as void extended across the via/metal line interface. Long reservoir effects appeared due to the supply of enough Al atoms from the reservoir region, which compensated the electromigrated Al atoms. Therefore, longer reservoir resulted in better electromigration reliability. As mentioned earlier, dominant mechanism of void formation at reservoir region seemed to be that vacancies generated by flux divergence near the W/Al interface diffused toward regions of lower vacancy concentration (i.e., reservoir region) due to the spatial gradient of vacancy concentration at relatively high temperature (200 °C in this work) [3–5]. Although global joule heating was negligible (under 5 °C) by low current density of 2 MA/cm^2 used in this experiment, local joule heating effects [5] near sharp corner of Al/W interface could induce higher temperature (and also, higher vacancy

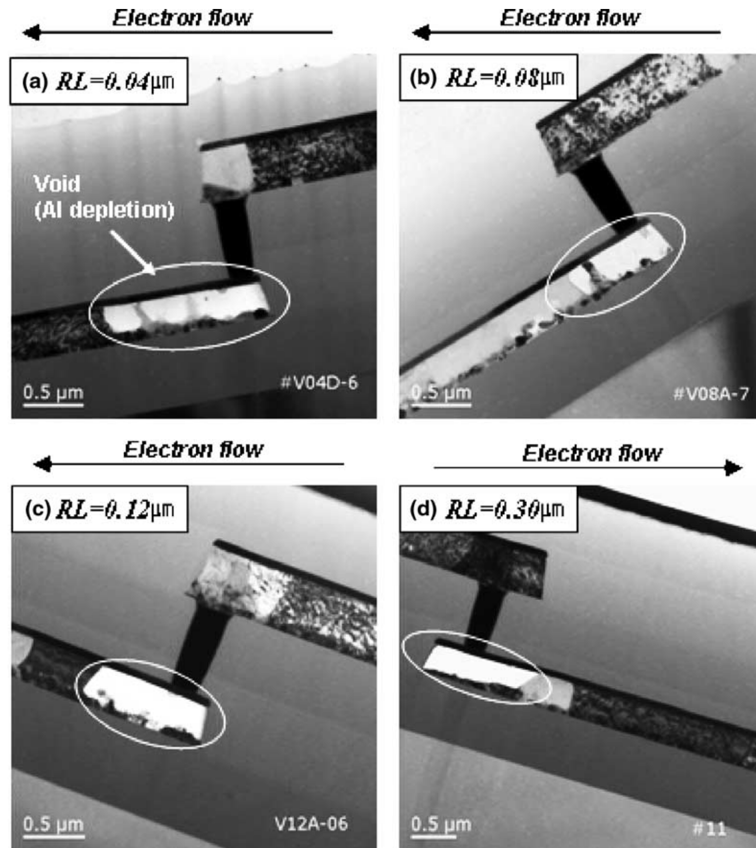

Fig. 4. Cross-sectional TEM photograph of metal 1 line end region of cathode direction after 20% resistance increase for FSG ILD with metal 1 reservoir length (RL) of (a) 0.04, (b) 0.08, (c) 0.12, and (d) 0.30 μm.

concentration) gradient between this current path region and reservoir region, which could enhance vacancy diffusion to reservoir region (or, equivalently, Al atom diffusion from reservoir region). In addition to these effects, it should be considered the effect of mechanical stress evolution on void formation in reservoir region during electromigration test, which will be discussed in the following sections.

3.2. Measurements of young's modulus and stress of dielectrics and interconnects

It is very important to know mechanical properties of each material in multilevel metallization structure to understand the effect of mechanical stress evolution on void formation in reservoir region during electromigration test. Young's modulus and residual stress of every constituent layer used in this test structure (cf. Fig. 1) were measured with a blanket film of 450 nm thickness by nanoindentation and wafer curvature method, respectively. Young's modulus was averaged from each measured value at five different sample positions. Fig. 5 showed the measured Young's modulus data of in-depth direction for each ILD material and Table 1 summarized material properties including measured Young's modulus for each material, which will be used for finite element modeling. Fig. 6 compared measured Young's modulus, measured residual stress, and coefficient of thermal expansion (CTE) which was taken from [2, 7–9] between FSG and FOX. It could be seen that FSG was relatively stiff and was under compressive stress while FOX was opposite.

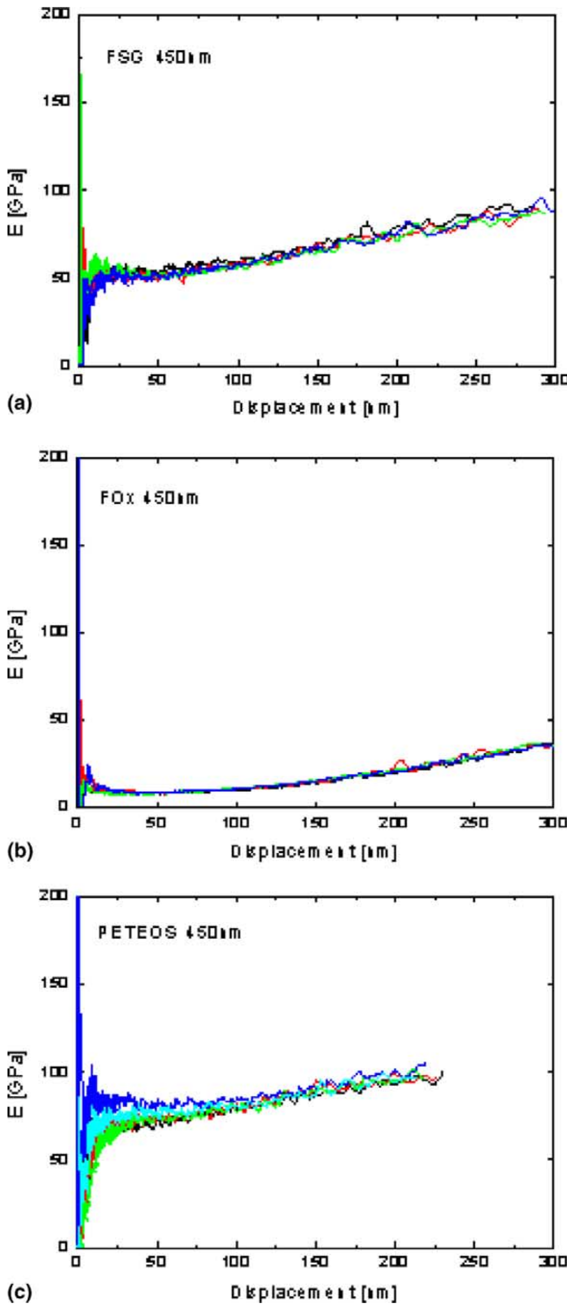

Fig. 5. Young's modulus with in-depth displacement at five different sample positions measured by nanoindentation method for 450 nm of (a) FSG, (b) FOX, and (c) PETEOS.

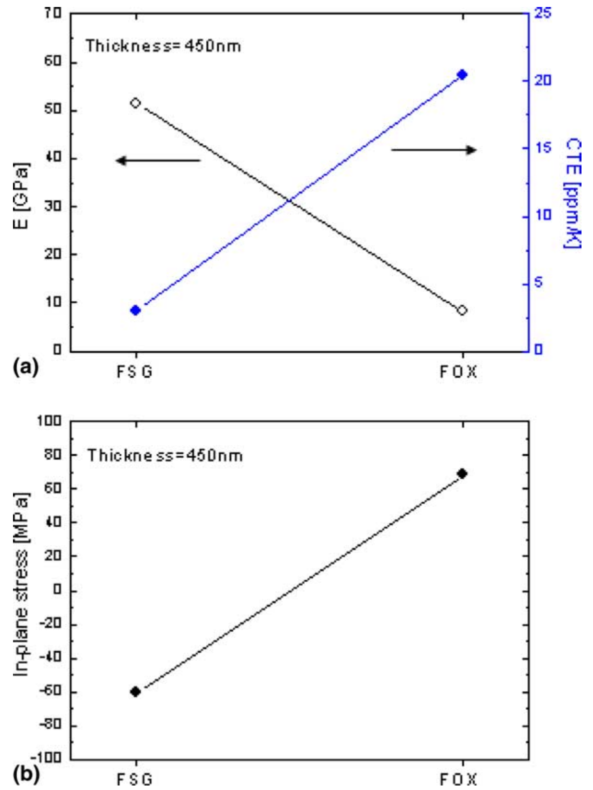

Fig. 6. Comparison of (a) Young's modulus (E), coefficient of thermal expansion (CTE), and (b) residual stress for 450 nm thick blanket film between FSG and FOX.

Residual stress measurement of Al–Cu interconnects using XRD method requires knowledge of the lattice spacing of Al–Cu film without stress [14,15]. Due to the strong (1 1 1) texture of Al–Cu film, especially, on Ti underlayer [12], only two different type {4 2 2} planes, used commonly, near the $\sin^2 \Psi$ of 0.11 and 0.78 could be observed, where Ψ indicates the angle from the sample normal to the normal of a diffracting plane [14,15]. Lattice spacing of Al {4 2 2} plane without stress (d_0) was obtained from two non-patterned Al films either with or without Ti underlayer, which resulted in different stress states of Al film. Measured d_0 was 0.0826654 nm that agrees well with the reported results [11,15]. We measured {4 2 2} lattice spacing of Al interconnect passivated by either FOX or FSG along the parallel and perpendicular directions of a dense array of straight Al lines. Cross-sectional scanning electron microscope (SEM) photograph of Al interconnects passivated by either FOX or FSG of 450 nm thickness was shown in Fig. 7. There was no void between metal

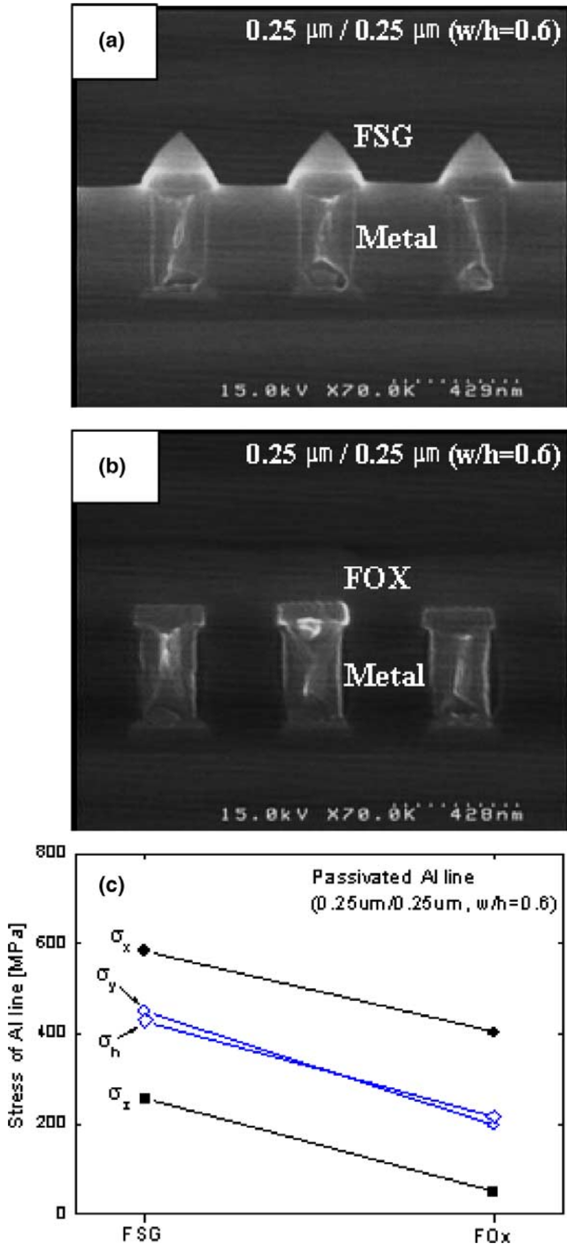

Fig. 7. Cross-sectional SEM photograph of a series of parallel Al lines passivated by either (a) FSG or (b) FOX, and (c) is the XRD measured triaxial stress components and hydrostatic stress of passivated Al lines.

lines in both cases and there were discrete differences in deposition profiles between FOX and FSG, which were mainly caused by their different deposition methods [11,17]. From these XRD experimental results, triaxial components of lattice spacing (d), strain (ε), and stress (σ) of Al interconnect passivated by either FSG or FOX were obtained in length (x), width (y), and height direction (z), separately. Detailed procedures to calculate Al interconnect stress were explained in several references [11,14,15]. Fig. 7 compared the measured triaxial stress components ($\sigma_x, \sigma_y, \sigma_z$) and hydrostatic stress ($\sigma_{\rm h} = (\sigma_x + \sigma_y + \sigma_z)/3$) of Al interconnect between FSG and FOX passivation where hydrostatic stress was usually associated with the stress-induced voiding [1,2]. In case of blanket Al film, it is usually in biaxial stress-state since there is no constraint in the normal direction. Unpassivated Al lines are close to uniaxial stress-state for narrower line width. Adding passivation dielectric increases Al interconnect stress due to the increased constraint in the normal direction, which results in a triaxial (or, hydrostatic) stress state in the metal line [9]. This hydrostatic stress requires a volume change in order to be reduced and drives the void formation and growth that can lead to interconnect failures [1,2]. Fig. 7 showed that all components of interconnect stress were larger for FSG than FOX. Although two passivation materials differed in CTE, residual stress, and stiffness (cf. Fig. 6), stiffness effect dominated, i.e., Al interconnect stress increased with increasing passivation stiffness, as discussed in detail at several references [9–11,21]. Therefore, the higher electromigration resistance of interconnects passivated by FOX than those passivated by FSG (cf. Fig. 3) could be best explained by the large stiffness difference which caused different constraint in the Al line during the electromigration when mechanical stresses and stress gradients were building up.

3.3. Finite element modeling on stress and vacancy concentration distributions

In order to investigate the effects of mechanical stress evolution on the void formation in the reservoir during electromigration test, we will consider only thermal stress by temperature excursion with neglecting electric current flow along metal line in our model structure. Distributions of ther-

mal stress and vacancy concentration near the reservoir region were calculated with variations of metal 1 reservoir length by 0.04, 0.08, 0.12, and 0.30 μm (cf. Figs. 1 and 2) using ABAQUS program and mathematical calculation, respectively. Al–Cu was assumed to behave as a temperature-dependent elastic–plastic material while the other layers were assumed to be linear elastic, as shown in Table 1. Among the various stress parameters [18], including von-Mises stress, principal stress, and hydrostatic stress, hydrostatic stress is the best indicator to investigate the stress-induced voiding phenomenon [1,2]. Fig. 8 showed some representative results on hydrostatic stress distribution around the metal 1 reservoir of 0.30 μm length for either FOX\PETEOS or FSG\PETEOS ILD structure at 200 °C. In common, both top-TiN and bottom-$TiAl_3$ layers of Al stack showed the

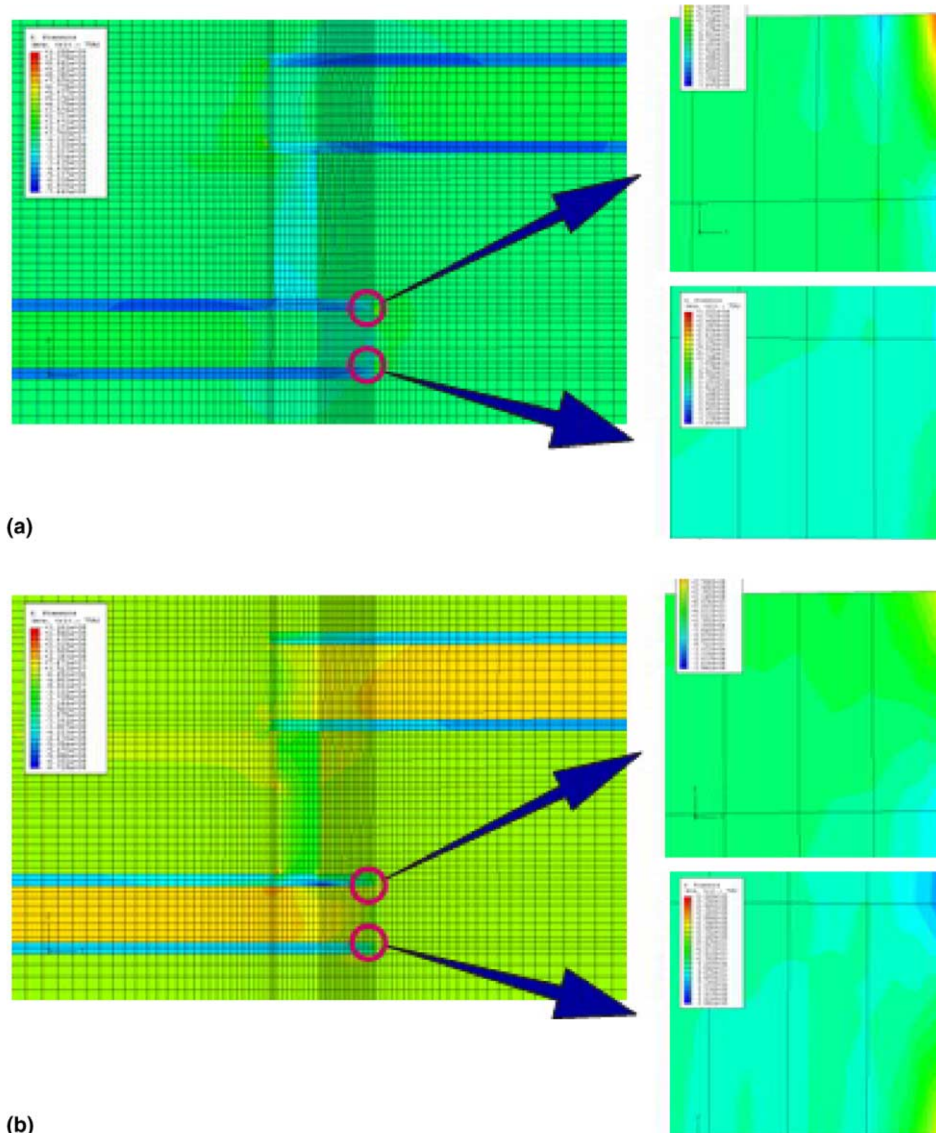

Fig. 8. Calculated distributions of hydrostatic stress around metal 1 reservoir of 0.30 μm length for (a) FSG\PETEOS and (b) FOX\PETEOS ILD structure at 200 °C.

highest stress levels by their high stiffness relative to low stiffness of in-between Al layer. Al layer had nearly uniform low-level stress along the metal line except the top and bottom corner regions where the singular stress developed, as shown in Fig. 8. Al with FSG showed a small tensile hydrostatic stress while Al with FOX showed a small compressive hydrostatic stress at 200 °C. There was no distinct difference in stress distribution in the reservoir with reservoir length variations from 0.04 to 0.30 μm for either FOX or FSG ILD structure. Our 2D plane strain analysis is thought to be reasonable in comparison to 3D full analysis because the narrow metal line is embedded in much wider dielectric layer and also the applied loading is the only uniform temperature change in whole structure.

It is well known that the equilibrium vacancy concentration, c_e, in the presence of stress has the form [19,20]

$$c_e = c_0 \exp((1-f)\Omega\sigma_h/kT), \quad (1)$$

where f is the average vacancy relaxation factor ($\sim$0.6), Ω the atomic volume (1.68×10^{-23} cm^3 for Al), σ_h the hydrostatic stress, k Boltzman's constant (8.62×10^{-5} eV/K), T the temperature

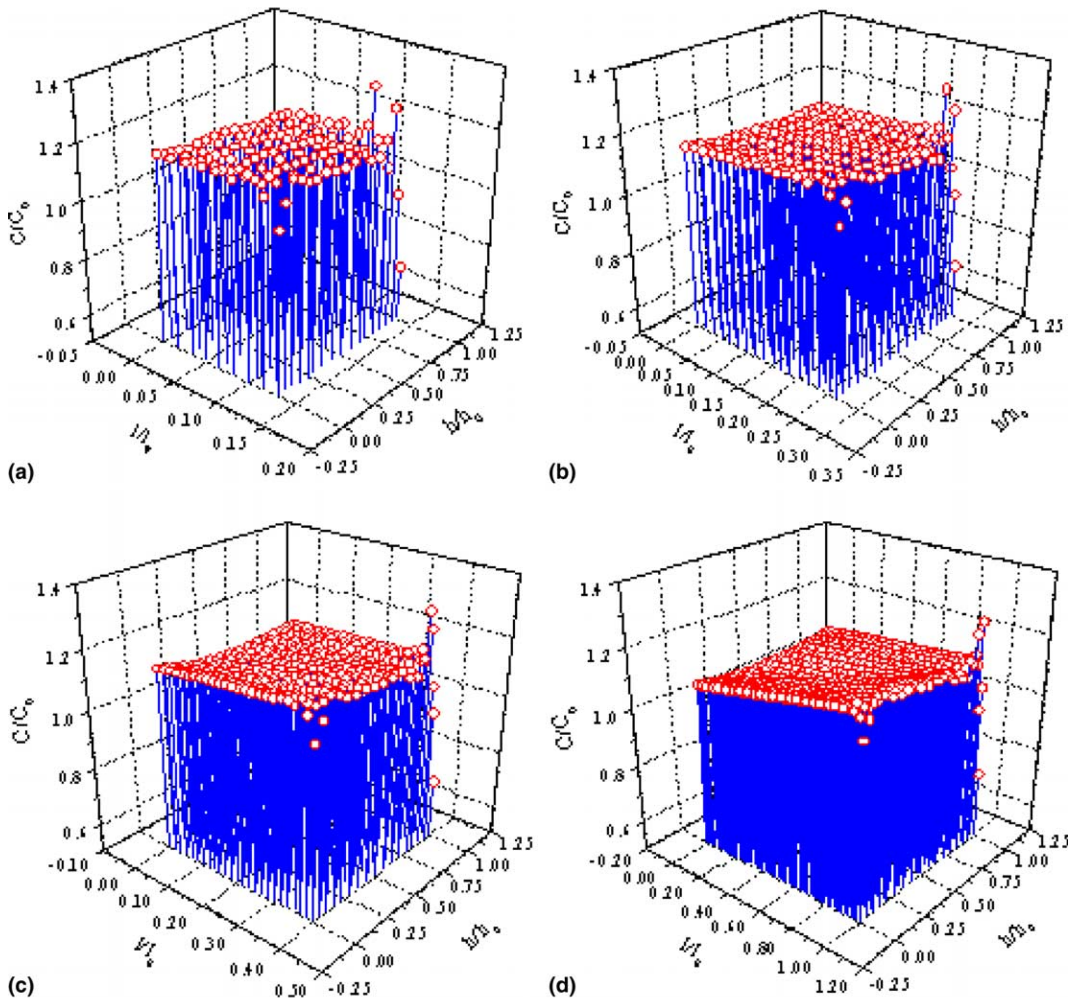

Fig. 9. Calculated distributions of equilibrium vacancy concentration in the metal 1 reservoir at 200 °C for FSG ILD with metal 1 reservoir length of (a) 0.04, (b) 0.08, (c) 0.12, and (d) 0.30 μm.

(200 °C: electromigration test temperature), while c_0 is the equilibrium vacancy concentration in the absence of stress (1.37×10^{19} cm^{-3} at ~200 °C for Al) [20]. Because there was no current flow in the reservoir during the electromigration test, it could be ignored the rate of vacancy concentration, $\partial c/\partial t$, and the reaction rate, G, which described the annihilation or production of vacancies for this case [20]. Hence, we considered this problem as a steady state one. Distributions of c_e in the reservoir, therefore, could be easily obtained from the calculated σ_h in the reservoir and the Eq. (1). Eq. (1) considered only the thermal stress effects on the equilibrium vacancy concentration distributions in the reservoir because there was no electric current flow in the reservoir although this assumption might be less realistic by neglecting vacancy generation phenomena near via/metal line interface induced by electric current flow. Analysis considering simultaneously both electromigration-induced and also thermal stress-induced vacancy formation would give more realistic results on the voiding mechanism in the reservoir during electromigration test. Figs. 9 and 10 showed the equilibrium vacancy concentration distributions in the reservoir at 200 °C with the variations of

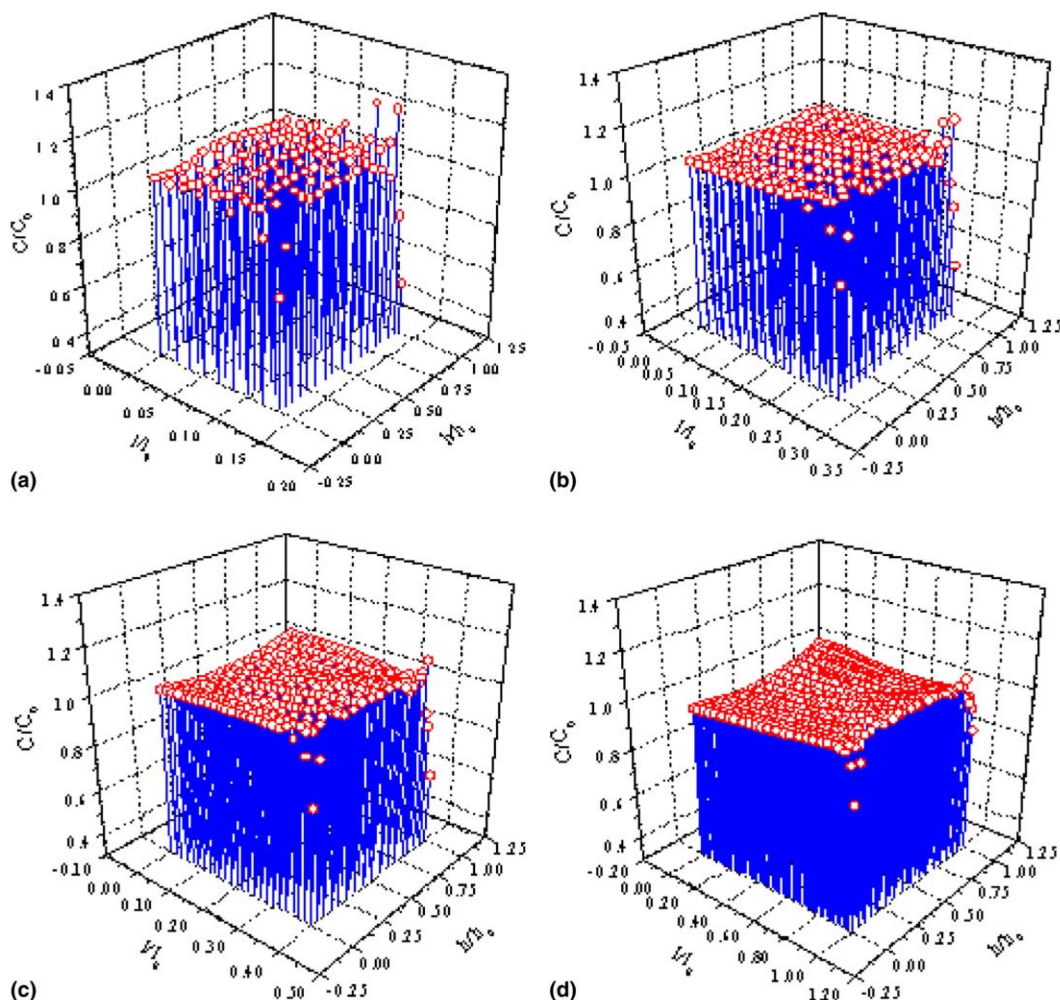

Fig. 10. Calculated distributions of equilibrium vacancy concentration in the metal 1 reservoir at 200 °C for FOX ILD with metal 1 reservoir length of (a) 0.04, (b) 0.08, (c) 0.12, and (d) 0.30 μm.

reservoir length for FSG and FOX, respectively. Here, c_e, reservoir length (l), and reservoir height (h) were normalized by c_0 ($= 1.37 \times 10^{19}$ cm^{-3}), l_0 ($= 0.3$ μm: maximum reservoir length), and h_0 ($= 0.3$ μm: Al thickness excluding bottom-$TiAl_3$ and top-TiN, cf. Fig. 1), respectively. It is noteworthy that c_e/c_0 over 1 means tensile σ_h while c_e/c_0 under 1 means compressive σ_h. More detail distributions of σ_h in the reservoir area could be seen from Fig. 9 (or 10) rather than Fig. 8. In common, it showed nearly uniform stress or vacancy concentrationdistribution in the reservoir area except the top and bottom corners of Al line where the singular distributions were developed. It was clear that Al reservoir with FSG was under a small tensile hydrostatic stress (or, c_e/c_0 over 1) while Al reservoir with FOX a small compressive hydrostatic stress (or, c_e/c_0 under 1). Both stress and vacancy concentration in the Al reservoir for FOX were lower than that for FSG at 200 °C, which were in consistent with the result that XRD measured interconnect stress for FOX was lower than that for FSG at room temperature, as shown in Fig. 7. Singularities near reservoir corner for FOX were also smaller than that for FSG. It was thought that effect of thermal conductivity difference between FOX and FSG on electromigration reliability would be negligible because the measured joule heating of Al interconnect for both ILD materials was just under 5 °C at our test condition (2 MA/cm^2 and 200 °C). It could be seen from Figs. 9 and 10 that both overall concentration and near-corner singularities decreased a little with the increase of reservoir length for either FSG or FOX. This meaned that Al stress in reservoir did not change much for its length variations. It was understood that dominant mechanism of void formation in the reservoir seemed to be that vacancies induced by atomic flux divergence near W/Al interface diffused toward regions of lower vacancy concentration (i.e., reservoir) due to spatial gradient of vacancy concentration. Longer reservoir supplied more Al atoms by the larger volume which compensated the electromigrated Al atoms, which resulted in longer electromigration lifetime for longer reservoir (cf. Fig. 3). It could be seen that effects of reservoir length variations on either thermal stress or stress-induced vacancy concentration were not significant. Therefore, interconnect structure with longer reservoir had better electromigration reliability dominantly due to the supply of more Al atoms from the reservoir region by the spatial gradient of vacancy concentration. Figs. 9 and 10 also showed that equilibrium vacancy concentrations increased as approaching to the reservoir edge. This means that reservoir end regions easily tend to nucleate void by the generated thermal stress.

4. Conclusions

Systematic experimental and computational analyses were conducted to investigate the effects of reservoir length (0.04–0.30 μm) and passivation material (FOX vs. FSG) on not only the distributions of both stress and vacancy concentration in reservoir but also the electromigration reliability of multilevel interconnect structure. The electromigration test results were mainly analyzed by both XRD and FEM for determination of the mechanical stress in the metal interconnects. Also, the mathematical calculations for the vacancy concentration distribution in reservoir were utilized. Stiffer ILD led to not only higher interconnect stress but also worse electromigration reliability due to the large constraint difference in metal line during the electromigration when mechanical stresses and stress gradients were building up. Multilevel interconnect with longer reservoir led to better electromigration reliability mainly due to the supply of more Al atoms by the spatial gradient of vacancy concentration while the effect of reservoir length variations on either thermal stress or stress-induced vacancy concentration in reservoir was not significant.

References

[1] L.T. Shi, K.N. Tu, Appl. Phys. Lett. 65 (1994) 1516.
[2] L.T. Shi, K.N. Tu, J. Appl. Phys. 77 (1995) 3037.
[3] M. Fujii, K. Koyama, J. Aoyama, Proc. VLSI Multilevel Interconnection Conf., Santa Clara, CA, IEEE, 1996, p. 312.
[4] Y. Kakuhara, S. Chikaki, Proc. Stress Induced Phenomena in Metallization, Tokyo, Japan, AIP, 1998, p. 89.
[5] S. Shingubara, T. Osaka, S. Abdeslam, H. Sakue, T. Takahagi, Proc. Stress Induced Phenomena in Metallization, Tokyo, Japan, AIP, 1998, p. 159.

[6] B. Greenebaum, A.I. Sauter, P.A. Flinn, W.D. Nix, Appl. Phys. Lett. 58 (1991) 1845.
[7] Y.L. Shen, J. Appl. Phys. 82 (1997) 1578.
[8] A. Gouldstone, Y.L. Shen, S. Suresh, C.V. Thompson, J. Mater. Res. 13 (1998) 1956.
[9] A.I. Sauter, W.D. Nix, IEEE Trans. Comp. Hybrids Manufact. Technol. 15 (1992) 594.
[10] S. Lee, J.C. Bravman, P.A. Flinn, T.N. Marieb, Proc. Stress Induced Phenomena in Metallization, Tokyo, Japan, AIP, 1998, p. 277.
[11] Y.P. Kim, D.C. Kwon, H.M. Choi, Y.W. Park, S.I. Lee, Proc. International Interconnect Tech. Conf., Burlingame, CA, IEEE, 2000, p. 205.
[12] Y.B. Park, D.W. Lee, Mater. Sci. Eng. B 87 (2001) 70.
[13] W.C. Oliver, G.M. Pharr, J. Mater. Res. 7 (1992) 1564.
[14] B.M. Clemens, J.A. Bain, MRS Bull. (July) (1992) 46.
[15] G. Cornella, S.H. Lee, W.D. Nix, J.C. Bravman, Appl. Phys. Lett. 71 (1997) 2949.
[16] ABAQUS User's Manual, Ver. 6.0, Hibbit, Karlson and Sorensen, Inc., Pawtucket, RI, 1999.
[17] Y.B. Park, J.Y. Kim, D.W. Seo, W.G. Lee, J. Electrochem. Soc. 148 (2001) G572.
[18] G.E. Dieter, Mechanical Metallurgy, McGraw-Hill, New York, 1986, p. 46.
[19] M.A. Korhonen, P. Borgesen, K.N. Tu, C.Y. Li, J. Appl. Phys. 73 (1993) 3790.
[20] M.E. Sarychev, Y.V. Zhitnikov, L. Borucki, C.L. Liu, T.M. Makhviladze, J. Appl. Phys. 86 (1999) 3068.
[21] Y.B. Park, I.S. Jeon, Microelectron. Eng. 69 (2003) 26.